

Reduced fluctuations in high confinement plasmas at negative triangularity on DIII-D

A. Marinoni¹, M.E. Austin², M.L. Walker³, E.M. Davis¹, A.W. Hyatt³, C.J. Lasnier⁴, C.C. Petty³, M. Porkolab¹, J.C. Rost¹, O. Sauter⁵, K.E. Thome³ and the DIII-D Team

¹ MIT Plasma Science and Fusion Center, Cambridge MA 02139 USA

² University of Texas at Austin, Austin TX 78705 USA

³ General Atomics, San Diego CA 92121 USA

⁴ Lawrence Livermore National Laboratory, Livermore CA 94550 USA

⁵ Swiss Plasma Center, EPFL, Lausanne 1015 CH

Plasmas with negative triangularity (δ) shape have been created on the DIII-D tokamak that are characterized by enhanced confinement and reduced fluctuations as compared to matched discharges at positive triangularity.

This work was inspired by previous results on the TCV tokamak [1], where the energy confinement time of collisionless, inner wall limited L-mode plasmas subject to pure electron heating was shown to double when reversing δ with other parameters held fixed. The DIII-D experiments investigated negative δ plasmas and their fluctuations using both pure electron (EC) and mixed ion-electron (EC-NBI) heating, thus exploring for the first time a more reactor relevant regime where $T_e \simeq T_i$. Compared to positive δ plasmas with the same elongation, current, density, toroidal field and auxiliary power, plasmas at negative δ feature lower heat diffusivities, which results in higher stored energy in both heating regimes. The intensity of density fluctuations monitored by the Phase Contrast Imaging diagnostic [2] is found to decrease at negative δ in both heating regimes, consistent with the increased confinement.

These experiments confirm early results on TCV and, more importantly, indicate that negative triangularity shape is also beneficial for confinement in a regime where the electron temperature is close to that of ions.

Effect of triangularity on confinement and fluctuations

The DIII-D tokamak has investigated the effect of negative δ shape on confinement and fluctuations by realizing inner-wall limited discharges with edge δ equal to -0.4. The poloidal cross

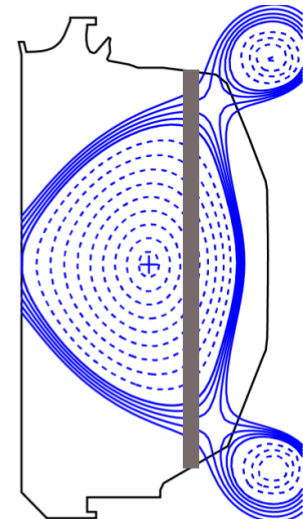


Figure 1: Reconstruction of the poloidal cross section for a typical negative triangularity discharge on DIII-D superimposed to the PCI line of sight.

section of a typical plasma is reported in Fig. 1, with the main parameters of the discharge being: current $I_p = 0.9\text{MA}$, toroidal field $B_T = 2\text{T}$, line-average density $\langle n_e \rangle = 3 - 5 \cdot 10^{19}\text{m}^{-3}$, elongation $\kappa = 1.33$, $q_{\text{lim}} = 4.3$; auxiliary heating was either pure ECH deposited just inside mid-radius, or a combined ECH-NBI, with $P_{\text{ECH}} = 3\text{MW}$ and $P_{\text{NBI}} = 3\text{MW}$. In order to quantitatively compare the effect of triangularity on transport, discharges at positive δ were carried out with matched B_T , I_p , κ , and auxiliary power but edge $\delta = +0.4$. The difference in the shape of the flux surfaces caused slight variations in quantities such as volume and toroidal flux, which increase by 3 – 8% in the negative δ discharges as compared to the positive δ counterparts. Larger discrepancies in the safety factor are found near the edge, with positive δ discharges featuring $q_{\text{lim}} \simeq 5$. The experiment compared discharges with matched shape and actuators such as plasma current, toroidal field and auxiliary power rather than dimensionless parameters in order to simulate the comparison of operational regimes of a fusion device with fixed power and field capabilities; a careful, and shot demanding, experimental plan could have been devised to match volume and safety factor in an effort to eliminate their impact on transport coefficients, but would have caused differences in the actuators.

The auxiliary heating was typically divided in an early EC-only phase, with sporadic torque balanced beam blips to allow the measurement of ion pressure and velocity profiles, followed by a combined EC-NBI heating phase; during the former phase the on-axis electron temperature was typically slightly below 3 keV and twice that of ions, while the latter phase features $T_e \simeq T_i$ across the entire radial profile and slightly above 3 keV on axis. In both phases the effective mid-radius inverse collisionality was about two. In the remainder of the paper we will focus on two discharges at opposite values of edge δ ($\delta_{\text{LCFS}} = -0.4$ and $\delta_{\text{LCFS}} = +0.4$) that have matched actuators throughout the entire shot length and the same line-average density in the ECH-only phase; both discharges operate with an L-mode edge and are thus free of ELMs.

During the ECH-only phase both discharges feature closely matched electron density, ion temperature and toroidal velocity profiles, while the electron temperature is up to 20% higher for the discharge at $\delta_{\text{LCFS}} = -0.4$, although nonuniformly across the radial profile. A reconstruction of the kinetic equilibrium with the EFIT code based on a ONETWO transport analysis shows that, by merely reversing the edge δ , the plasma stored energy content increases by about 25%. In the region $0.4 \leq \rho \leq 0.9$, where transport coefficients are reconstructed with acceptable confidence intervals, single-fluid effective diffusivities decrease by 20% – 35%.

In the combined EC-NBI heating phase we observe variations in all kinetic profiles: as compared to the discharge at $\delta_{\text{LCFS}} = +0.4$, the negative δ case features a 20% increase for on-axis electron density with about the same edge value, while T_e , T_i and v_ϕ are higher in the radial

region $0.4 \leq \rho \leq 0.9$, with cross-overs on axis and at the edge. A kinetic analysis shows that, even in this regime where $T_e \simeq T_i$, the effect of reversing δ causes the stored energy to increase by 30%, while single-fluid effective diffusivities decrease by 25% – 40% in the radial region $0.4 \leq \rho \leq 0.9$. It is worth mentioning that, since about 40% of the NBI power couples to electrons, even in this heating phase the plasmas are in an electron-flux dominated regime, despite the fact that the NBI system couples as much power as the EC system.

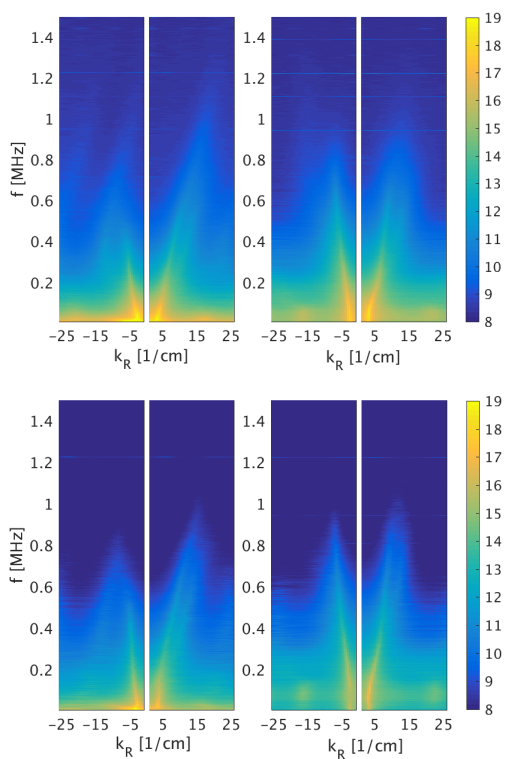


Figure 2: PCI frequency-wavenumber spectra, during the ECH-only (top) and the combined ECH-NBI (bottom) heating phases for (left) $\delta_{LCFS} = -0.4$ and (right) $\delta_{LCFS} = +0.4$.

The two dimensional wavenumber spectra, shown in Fig.2 normalized to the line average density along the line of sight, suggest that turbulence eddies might be tilted in different ways in the two shapes. Low-shear regimes such as L-mode typically create spectra symmetric in k_{\perp} , while highly-sheared H-mode edge typically create spectra asymmetric in k_{\perp} [3] such as those seen in the ECH-NBI phases; which would be consistent with the LORB5 code [1], which showed that the negative δ shape induces a poloidal tilt to turbulent eddies, resulting in larger k_{\perp} and reduced mixing-length diffusivities.

Macro and micro stability analysis

The kinetic equilibrium of the negative δ discharge during the mixed EC-NBI heating phase, which has higher β than during the EC-only phase, was used as a starting point for a pres-

The intensity of density fluctuations was monitored by the Phase Contrast Imaging diagnostic, which images line-integrated density fluctuations onto a linear array of detectors; the vertical line of sight is shown in Fig.1. The system is sensitive to scattering wavelets propagating in the horizontal laboratory plane in the range $1\text{cm}^{-1} \leq k_{\perp} \leq 25\text{cm}^{-1}$, and in the frequency range $10\text{kHz} \leq f \leq 2\text{MHz}$, with the lower cut-off set by a high-pass filter aimed at reducing the impact of mechanical vibrations on the measurements. In both heating phases, the intensity of density fluctuations is seen to decrease at all $f \geq 50\text{kHz}$ in the negative δ shape. A quantitative comparison of the rms values shows that the total intensity of fluctuations, normalized to the line-average density along the PCI line of sight, decreases by 25% and 15%, respectively, in the EC-only and EC-NBI heating phases.

The two dimensional wavenumber spectra, shown

sure scan aimed at predicting the β limit of such plasmas. Inverse equilibria were reconstructed at each step by the CORSICA code and provided as input to the MHD stability code GATO to predict the β limit. Since sawteeth are destabilized in these discharges, the β limit for the onset of an internal pressure driven kink mode was estimated with a method developed in [4] which, as a function of pressure, finds a threshold in the edge displacement. This method yielded a limit of $\beta_N \simeq 3.1$, which would be suitable in a reactor provided that the L-mode edge can be maintained.

Early non-linear local gyro-kinetic simulation of TCV discharges found that the increased confinement at negative δ was due to a weakening of Trapped Electron Modes, which were the dominant instability in those cases, due to a modification of the toroidal precession drift exerted by plasma shape [5]. A linear gyro-kinetic analysis of the discharges described in this paper finds that TEM modes are still the dominant ion-scale instability, consistent with the discharges being in an electron-flux dominated regime. Additionally, growth rates are seen, at various radii, to decrease with decreasing δ in the spectral region $k_\theta \rho_s \leq 1.5$. The plasmas described in this report, as opposed to the experiment on TCV, are predicted to suffer from significant electron-scale fluctuations due to the lower T_e/T_i ratio, which could partly explain why the fractional increase in confinement obtained by reversing δ is lower than what was observed on TCV.

Acknowledgement

The authors wish to thank Drs. A.D. Turnbull and F. Turco for valuable assistance with the GATO and CORSICA codes. This material is based upon work supported by the U.S. Department of Energy, Office of Science, Office of Fusion Energy Sciences, using the DIII-D National Fusion Facility, a DOE Office of Science user facility, under Awards DE-FC02-04ER54698, DE-FG02-94ER54235, DE-FC02-99ER54512 and DE-SC0016154. DIII-D data shown in this paper can be obtained in digital format by following the links at https://fusion.gat.com/global/D3D_DMP. Part of the data analysis was performed using the OMFIT framework.

References

- [1] Y. Camenen *et al.*, 2007 *Nucl. Fusion* **47** 510
- [2] J. Dorris *et al.*, 2009 *Rev. Sci. Instrum.* **80** 023503
- [3] J.C. Rost *et al.*, 2014 *Phys. Plasmas* **21** 062306
- [4] A.D. Turnbull *et al.*, 1999 *Nucl. Fusion* **39**, 1557
- [5] A. Marinoni *et al.*, 2009 *Plasma Phys. Control. Fusion* **51** 055016